Exploratory study of three-point Green's functions in Landau-gauge Yang-Mills theory

Attilio Cucchieri,* Axel Maas,† and Tereza Mendes‡

Instituto de Física de São Carlos, Universidade de São Paulo, Caixa Postal 369, 13560-970 São Carlos, SP, Brazil

(Received 16 May 2006; published 6 July 2006)

Green's functions are a central element in the attempt to understand nonperturbative phenomena in Yang-Mills theory. Besides the propagators, 3-point Green's functions play a significant role, since they permit access to the running coupling constant and are an important input in functional methods. Here we present numerical results for the two nonvanishing 3-point Green's functions in 3d pure SU(2) Yang-Mills theory in (minimal) Landau gauge, i.e. the three-gluon vertex and the ghost-gluon vertex, considering various kinematical regimes. In this exploratory investigation the lattice volumes are limited to 20^3 and 30^3 at $\beta = 4.2$ and $\beta = 6.0$. We also present results for the gluon and the ghost propagators, as well as for the eigenvalue spectrum of the Faddeev-Popov operator. Finally, we compare two different numerical methods for the evaluation of the inverse of the Faddeev-Popov matrix, the point-source and the plane-wave-source methods.

DOI: 10.1103/PhysRevD.74.014503 PACS numbers: 12.38.Aw, 11.10.Kk, 11.15.−q, 11.15.Ha

I. INTRODUCTION

The nonperturbative properties of Yang-Mills theory are still an open and challenging problem, especially the issue of confinement. Nonetheless, much progress has been made in their understanding over the decades. One central element in these investigations are Green's functions, which can describe a quantum field theory completely. In particular, their infrared behavior has been related to confinement: in two of the most popular scenarios of confinement, the Gribov-Zwanziger scenario [1–4] and the Kugo-Ojima scenario [5], a specific behavior is predicted for the 2-point Green's functions—the propagators—in Landau gauge.

According to these scenarios, the Faddeev-Popov ghost propagator should be enhanced in the infrared limit when compared to a massless-particle pole, while the gluon propagator should vanish. Calculations using functional methods agree with these predictions and have found that the propagators show a powerlike behavior in the far infrared region, with characteristic exponents. These results have been obtained using Dyson-Schwinger equations in various dimensions [3,6–8] and have been confirmed by renormalization group methods [9]. On the other hand, these methods rely on approximations concerning the higher n-point Green's functions, especially the three-point vertices. Thus, it is important to check explicitly whether the assumptions made for the vertices in these methods are justified. This has been done, again using functional methods, but as of yet only for specific momentum configurations of the n-point Green's functions and in the far infrared limit [10,11], or using further approximations [11,12]. In both cases the results are consistent with the assumptions made so far.

Numerical studies of lattice gauge theories also support the two confinement scenarios described above, confirming the infrared enhancement of the ghost propagator [13–16] and the suppression of the gluon propagator (in the 3d case) at low momenta [17,18]. Let us recall that, in order to probe the infrared limit, one needs to use very large lattice volumes. Recently, in four dimensions, investigations have been performed also considering (strongly) asymmetric lattices [19], in order to have access to small momenta while keeping the lattice volume relatively small. The results obtained show an infrared suppression of the gluon propagator. However, these simulations are affected by systematic effects [20,26], making it difficult to extract quantitative information from this type of lattices.

Let us stress that the agreement between the functional methods and the lattice data is still at the qualitative level. In particular, it is still not clear if the numerical data support a gluon propagator vanishing in the infrared [18,21]. Recent studies by functional methods [22] suggest nontrivial effects related to the use of discretized space-time on compact manifolds, which could be responsible for this discrepancy. Let us also recall that, in the continuum, a finite (nonzero) gluon propagator at zero momentum seems to be compatible with the Gribov-Zwanziger scenario only in the case of an infrared enhanced ghost-gluon vertex [23,24]. On the other hand, such an enhancement would be at variance with results from functional methods [10–12] and from recent lattice studies [25,26].

In this work we present an exploratory study of the Landau gauge three-gluon vertex and of the ghost-gluon vertex for various momentum configurations, in the three-dimensional pure SU(2) case. After this exploratory study we will be able to consider (for the interesting cases) very large lattice volumes and to probe the limit of small momenta. This is the first numerical study of these vertices in the three-dimensional case. Clearly, the 3d simulations are computationally less demanding than those in 4d and they may help to get a better understanding of the four-

*Electronic address: attilio@ifsc.usp.br
†Electronic address: axelmaas@web.de
‡Electronic address: mendes@ifsc.usp.br

dimensional case. Furthermore, results in three dimensions are of interest in their own right, as three-dimensional Yang-Mills theory is the (most relevant part of the) infinite-temperature limit of its four-dimensional counterpart [27]. In addition, a connection exists between 4d Yang-Mills theory in Coulomb gauge and 3d Yang-Mills theory in Landau gauge [11,28].

Let us note that previous lattice studies of these vertices in the 4d case [25,29–31] usually focused on specific momentum configurations, mostly with the aim of extracting the running coupling constant and for comparison to perturbative studies. In this preliminary work we use several kinematical configurations in order to test the numerical methods employed and to study the influence due to discretization and to finite-volume effects. In addition, we present results for the propagators and for the spectrum of the Faddeev-Popov operator, which plays an important role in the Gribov-Zwanziger scenario [1–4,32].

In Sec. II the technical details for the generation of the configurations, the gauge-fixing procedure and the error analysis are given. We report definitions and results for the propagators in Sec. III and for the vertices in Sec. IV. A summary and outlook conclude this work in Sec. V.

II. GENERATION OF CONFIGURATIONS

The action considered is the usual, unimproved Wilson action [33] for the SU(2) gauge group. Configurations are generated using a hybrid-over-relaxation (HOR) update, consisting of five over-relaxation [34] and one heat-bath sweeps. For the heat-bath update, a mixed Creutz [35] and Kennedy-Pendleton [36] algorithm is employed. The lattices have volumes $V = N^3 = 20^3$ and 30^3, and calculations have been performed at $\beta = 4.2$ and $\beta = 6.0$. We use 200 HOR updates for thermalization and 40 or 45 HOR updates between evaluation of the Green's functions. The results have been obtained in multiple independent runs using hot initial configurations.

For the extraction of the vertices, large statistics have been necessary. Table I lists the precise values. Also, the expectation value of the plaquette is given for each lattice volume and β value. The results are in agreement with [18,37]. The error on the plaquette is the statistical error including a correlation-time analysis. We always find that the integrated autocorrelation time [38] is less than 1 HOR sweep. Following Ref. [18] we also evaluate the inverse lattice spacing (in GeV).

The gauge fixing to Landau gauge has been performed using a stochastic-over-relaxation method [39] with a self-adapting acceptance probability. The condition for gauge fixing has been a test on the quantity [39]

$$e_6 = \frac{1}{d}\sum_{\mu}\frac{1}{N_\mu}\sum_{c}\frac{1}{[\mathrm{tr}(Q_\mu\sigma_c)]^2}\sum_{x_\mu}(\mathrm{tr}\{[q_\mu(x_\mu) - Q_\mu]\sigma_c\})^2, \tag{1}$$

which was required to be less than 10^{-12}. Here we use the definitions

$$q_\mu(x_\mu) = \frac{1}{2i}\sum_{x_\nu,\nu\neq\mu}[g(x)U_\mu(x)g(x+e_\mu)^\dagger - g(x+e_\mu)U_\mu(x)^\dagger g(x)^\dagger] \tag{2}$$

$$Q_\mu = \frac{1}{N_\mu}\sum_{x_\mu} q_\mu(x_\mu). \tag{3}$$

Also, $\{U_\mu(x)\}$ is a thermalized lattice configuration, $\{g(x)\}$

TABLE I. For each lattice volume V and coupling β we report here the average value of the plaquette $\langle P\rangle$, the inverse lattice spacing $1/a$ (in GeV), the number of independent runs and the number of configurations considered for the evaluation of propagators and vertices. The values of the plaquette, the data for the propagators and the eigenvalue spectrum (reported in Sec. III) have been obtained using the data set labeled *Propagators*. On the other hand, the propagators involved in the determination of the vertices have been determined considering the same data set as the corresponding vertex. Finally, note that the set labeled *Three-gluon vertex* includes all the configurations considered in the other two data sets.

				Propagators	
Volume	β	$\langle P\rangle$	$1/a$ [GeV]	Runs	Config.
20^3	4.2	0.741865(5)	1.136(8)	19	6161
30^3	4.2	0.741860(2)	1.136(8)	53	10229
20^3	6.0	0.824781(3)	1.733(8)	18	5777
30^3	6.0	0.824781(1)	1.733(8)	48	10099
		Ghost-gluon vertex		*Three-gluon vertex*	
Volume	β	Runs	Config.	Runs	Config.
20^3	4.2	19	6903	38	13064
30^3	4.2	36	11052	89	21281
20^3	6.0	17	7004	35	12781
30^3	6.0	16	11172	64	21271

represents the gauge transformation applied on the link variables $U_\mu(x)$, the symbol † indicates Hermitian conjugate, N_μ is the lattice side in the μ direction, d is the space-time dimension (3 in our case), e_μ is a positive unit vector in the μ direction and σ_c are the three Pauli matrices, normalized as $\sigma_c^2 = 1$. Both the link variables $U_\mu(x)$ and the gauge-transformation matrices $g(x)$ are elements of the $SU(N_c)$ group (in the fundamental $N_c \times N_c$ representation). In order to speed up the calculation, the quantity e_6 was not evaluated for each stochastic-over-relaxation sweep, but an adaptive-predictor method has been used for each configuration. Thus, in some cases we obtain for e_6 a value considerably smaller (by some orders of magnitude) than 10^{-12}. Nevertheless, we usually found for the quantity e_6 a final value between 10^{-12} and 10^{-13}. No results on Gribov-copy effects will be given in this exploratory study, but tests using relatively small statistics, i.e. generating 20 Gribov copies for each configuration and considering only a small subset of thermalized configurations, suggest that the effects are at the quantitative rather than at the qualitative level.

All errors given for the propagators and the vertices have been calculated using a standard bootstrap method with 1000 bootstrap samples. The quoted errors represent a 67% confidence interval.

Most of the results shown here have been obtained using a code developed independently from the one used in Ref. [18] (see also [40]). Nonetheless, when possible, we checked that results obtained with the two codes agree for propagators and vertices.

III. PROPAGATORS

A. Gluon propagator

The gluon propagator is given by the correlation function (see for example [15])

$$D^{ab}_{\mu\nu}(p) = \frac{1}{V}\langle A^a_\mu(p) A^b_\nu(-p)\rangle, \tag{4}$$

with the momentum-space lattice gluon field defined as [30]

$$A^a_\mu(p) = e^{-i\pi p_\mu/N} \sum_x \frac{e^{2\pi i p x/N}}{4i} \mathrm{tr}[(U_\mu(x) - U_\mu(x)^+)\sigma_a]. \tag{5}$$

Here the components p_μ of p get the integer values $-N/2+1, \ldots, N/2$ (for even lattice sides and for symmetric lattices with $N_\mu = N$). Note that we do not divide the Fourier transform of the gluon field by the lattice volume $V = N^3$.

As for the exponential prefactor $\exp(i\pi p_\mu/N) = \exp(i\pi p_\mu a/L)$, it allows one to obtain an improved lattice Landau gauge condition [30], i.e. the continuum condition $\partial \cdot A = 0$ is recovered with corrections $\mathcal{O}(a^2)$, instead of the corrections $\mathcal{O}(a)$ obtained when this prefactor is neglected. This exponent also appears naturally in a weak-coupling expansion of lattice gauge theory [41]. Note that this factor is a discretization correction. Indeed, it goes to 1 in the limit $a \to 0$ while keeping the physical lattice size $L = aN$ fixed. Furthermore, it is equal to 1 in the infrared limit $p \to 0$. This factor cancels when evaluating the scalar part of the gluon propagator [see Eq. (6) below], but in general not for vertices. An exception is e.g. the orthogonal configuration of the ghost-gluon vertex considered below (see Sec. IV). Numerical studies [30,42] have verified that this factor is also necessary in order to obtain the correct tensor structure of Green's functions involving gluon fields.

After contracting Eq. (4) with a transverse projector and a unit matrix in color space, the scalar part of the gluon propagator is given by

$$D(p) = \frac{1}{V\mathcal{N}} \sum_{\mu,a} \langle [\Re A^a_\mu(p)]^2 + [\Im A^a_\mu(p)]^2\rangle, \tag{6}$$

where $\Re A^a_\mu(p)$ and $\Im A^a_\mu(p)$ indicate, respectively, the real and the imaginary part of $A^a_\mu(p)$ and the normalization $\mathcal{N}$ is given by dN_c for $p > 0$ and by $(d-1)N_c$ for $p = 0$. The propagator is by definition inherently positive semidefinite. Let us recall that in minimal Landau gauge one has

$$\sum_\mu P_\mu A_\mu(p) = 0, \tag{7}$$

where the components of the physical momenta (denoted by capital letters when they are in lattice units) are given by

$$P_\mu = 2\sin\frac{\pi p_\mu}{N_\mu}. \tag{8}$$

Results will be presented as a function of the magnitude of the physical momentum $p = |P|/a$ (in GeV). Note that, with our notation, the continuum gluon propagator is obtained considering the product $\beta a^2 D(k)$. Indeed in d dimensions one has $\beta = 2N_c/(g^2 a^{4-d})$. Also, with $N_c = 2$, the lattice quantity $2A^a_\mu(x)/(ga) = \sqrt{\beta/a^{d-2}} A^a_\mu(x)$ goes to the continuum quantity $A^a_\mu(x)$ in the formal continuum limit $a \to 0$. In the same limit, $\sqrt{\beta a^{d+2}} A^a_\mu(p)$ converges to the continuum momentum-space gluon field $A^a_\mu(p)$. Thus, for any dimension d, the lattice quantity $\beta a^2 D(k)$ converges to the continuum gluon propagator in momentum space.

It is necessary to evaluate the gluon propagator for various momentum configurations in order to determine the vertices. In addition, some extra momentum configurations have been considered to check effects related to the breaking of rotational invariance. The various kinematical configurations are given in Table II. Let us note that, in general, for a given momentum p one has $A^a_\mu(p) \neq A^a_\nu(p)$, when $\mu \neq \nu$. For example, if the momentum is aligned along the μ-direction, then $A^a_\mu(p)$ vanishes for each color

TABLE II. Kinematical momentum configurations considered for the propagators. The columns *Gluon* and *Ghost* identify whether these configurations have been used for the evaluation of the propagators. The columns n_x, n_y and n_z give the components of the momentum. The *Type* is used for later identification of classes of momenta. The quantities $p_{\min}$ and $p_{\max}$ (in MeV) are the smallest and the largest momenta. The smallest momentum is evaluated at $\beta = 4.2$, while the largest is evaluated at $\beta = 6.0$ (in both cases we used the 30^3 lattice volume). The variables n and m run independently over all possible positive integer values $0, \ldots, N/2$ (but for the ghost propagator one cannot consider the zero momentum case).

Type	n_x	n_y	n_z	$p_{\min}$	$p_{\max}$	*Gluon*	*Ghost*
Plane	n	m	0	238	4902	$\surd$	$\surd$
Plane	n	$-n$	0	336	4902	$\surd$	
Plane	$-n$	0	n	336	4902	$\surd$	$\surd$
Plane	0	n	$-n$	336	4902	$\surd$	$\surd$
Diagonal	n	n	n	411	6004	$\surd$	$\surd$

component due to the relation (7) or, equivalently, due to the constancy of the quantity $q_\mu(x_\mu)$ defined in Eq. (2).

The results for $D(p)p^2$ and $D(p)$ are shown in Fig. 1 for the 30^3 lattice volume and the two β values considered. The statistical errors are below 1%, thus systematic errors are clearly visible. In particular, violation of rotational symmetry is the dominant effect and is of the order of several percent. In addition, finite-physical-volume effects are visible, especially in the far infrared, when going from $\beta = 4.2$ to $\beta = 6.0$. The latter effect is much more pronounced for the 20^3 lattices. Altogether, the systematic errors are the dominating effect at this level of statistics.

At the largest momentum (for $\beta = 6.0$) the propagator is about 6% or 5.5% larger than its resummed one-loop perturbative value [8] (which itself deviates from the tree-level value by about 3.5%) on the 20^3 and the 30^3 lattices, respectively. This discrepancy cannot be explained by removing tadpole contributions from the definition of the gluon field (see for example [15]). Indeed, if we consider [43] the gauge invariant definition of the tadpole factor given by $u_0 = \langle P \rangle^{1/4}$, where $\langle P \rangle$ is the average value for the plaquette, we find (see Table I) that the gluon propagator is multiplied by $1/u_0^2 \approx 1.1610$ at $\beta = 4.2$ and by $1/u_0^2 \approx 1.1011$ at $\beta = 6.0$. This clearly enhances the discrepancy between the data and the resummed leading-order perturbation theory. On the other hand, one should recall that, by changing the lattice discretization for the gluon field (see for example [44] and references therein), one finds a gluon propagator that differs by a global multiplicative constant. In particular, one can easily find definitions of the gluon field for which the gluon propagator is sensibly smaller than that obtained with the standard definition (see for example Table 1 in Ref. [45]). Of course, different lattice discretizations converge to a common result as the continuum limit is approached [45].

Finally, we note that the combinations of lattice size and β values considered here are not sufficient to reach the infrared regime, where the bending over of the propagator has been observed [18]. Nevertheless, one clearly sees

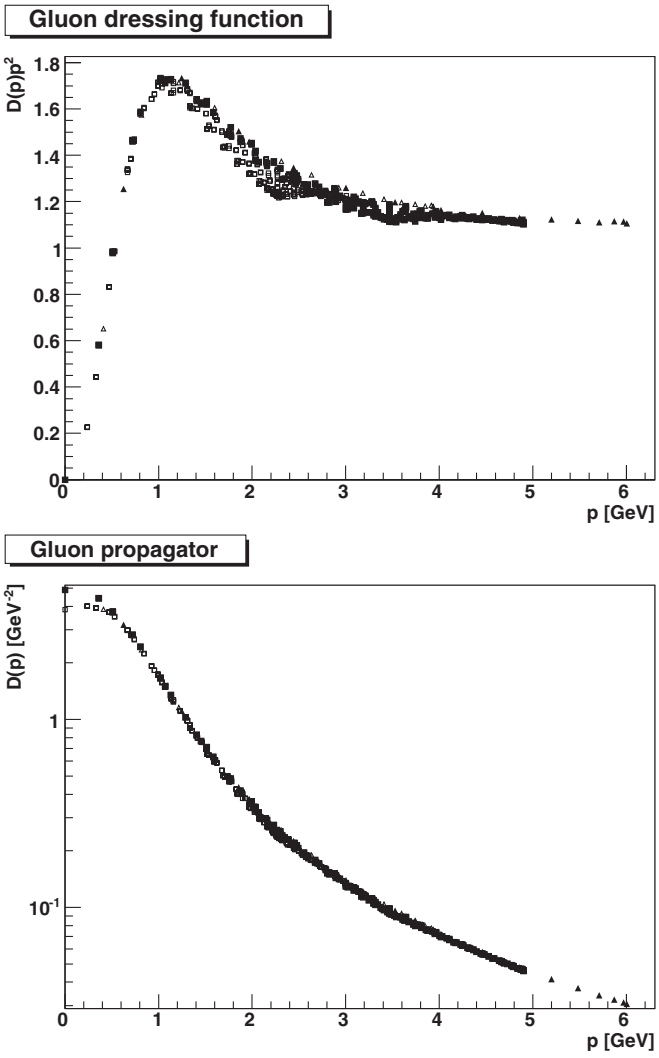

FIG. 1. The gluon dressing function $D(p)p^2$ (top) and the gluon propagator $D(p)$ (in GeV^{-2}, bottom) as a function of p (in GeV). Open and full symbols correspond, respectively, to $\beta = 4.2$ and to $\beta = 6.0$. In both cases we consider the lattice volume $V = 30^3$. Squares and triangles correspond to plane and diagonal momentum configurations, respectively.

from Fig. 1 that the propagator is less singular than $1/p^2$ for momenta smaller than about 1 GeV.

B. Ghost propagator

The numerical evaluation of the ghost propagator is considerably more complicated than that of the gluon propagator. Indeed, one has to evaluate

$$D_G^{ab}(p) = \frac{1}{V}\langle (M^{-1})^{ab}(p)\rangle, \tag{9}$$

where $M^{ab}(x, y)$ is the Faddeev-Popov operator, defined in the continuum as

$$-\partial_\mu D_\mu^{ab} = \delta(x-y)(-\partial^2\delta^{ab} + g f^{abc}\partial_\mu A_\mu^c). \tag{10}$$

Here f^{abc} are the structure constants of the $SU(N_c)$ gauge group. In Landau gauge, on the lattice, this operator is a matrix (with color and space-time indices), defined by its action on a scalar function $\omega^b(x)$ (with color index b) as [2]

$$\begin{aligned} M^{ab}(x, y)\omega^b(y) = \delta_{xy}\sum_\mu \Big\{ & G_\mu^{ab}(y)[\omega^b(y) - \omega^b(y + e_\mu)] \\ & - G_\mu^{ab}(y - e_\mu)[\omega^b(y - e_\mu) - \omega^b(y)] \\ & + \sum_c f^{abc}[A_\mu^b(y)\omega^c(y + e_\mu) \\ & - A_\mu^b(y - e_\mu)\omega^c(y - e_\mu)]\Big\}. \end{aligned} \tag{11}$$

Here, the sum over repeated indices (y and b) is understood and $G_\mu^{ab}(x)$ is given by

$$G_\mu^{ab}(x) = \frac{1}{8}\,\mathrm{tr}(\{\sigma_a, \sigma_b\}[U_\mu(x) + U_\mu(x)^+]), \tag{12}$$

i.e. it is proportional to δ^{ab}. Let us recall that in minimal Landau gauge [2] the gauge-fixed configurations are inside the first Gribov horizon, implying that the Faddeev-Popov operator $M^{ab}(x, y)$ is symmetric and positive (in the subspace orthogonal to the trivial and constant zero modes).

In order to evaluate the Fourier transform of the inverse operator[1]

$$(M^{-1})^{ab}(p, q) = \sum_{x,y} e^{2\pi i(px+qy)/N}(M^{-1})^{ab}(x, y) \tag{13}$$

the matrix inversion has been performed using the point source $\delta^{ac}(\delta_{x0} - 1/V)$ (see Ref. [46]). Compared to the inversion using a plane-wave source [47], this method has the advantage of only $N_c^2 - 1$ inversions per configuration, independently of the number of momenta, instead of $N_c^2 - 1$ inversions per configuration and for each momentum considered. However, as we will see below, statistical fluctuations are significantly enhanced at large momenta [46]. Also, note that this procedure is ambiguous with respect to the sign of the resulting propagator[2] (or of the eigenvalues). Thus, the sign has to be assigned by hand.

Since the Faddeev-Popov operator $M^{ab}(x, y)$ is symmetric and positive, the matrix inversion can be performed using a conjugate-gradient (CG) method (see for example [48]). From the numerical point of view, there are two issues to be careful about. First of all, as finite-precision arithmetic is used, it is possible for the solution to develop a component along the (constant) zero modes of the Faddeev-Popov operator. Thus, it is necessary to reorthogonalize the solution at each CG iteration with respect to this subspace.

The second aspect is related to the convergence of the CG method. Indeed, in finite precision arithmetic, the CG method normally loses orthogonality to the Krylov subspace already spanned. Thus, the magnitude of the residual can be incorrect. To compensate for this, an additional, albeit technical, quality criterion can be considered (see [48] Sec. 5.3 for details). As a convergence test, we check if the average of the components of the residual is less than 10^{-12} and if the additional quality parameter[3] is less than 10^{-13} between two CG iterations. This is usually achieved after several tens to a few hundreds of iterations. We have also checked that much weaker convergence tests do not change the propagators by more than a few percent. Let us note that one CG inversion of the Faddeev-Popov matrix is much faster than the gauge-fixing procedure when considering large lattice volumes.

The results for the color-averaged diagonal ghost propagator are shown in Fig. 2 for the lattice volume $V = 30^3$. Again, the statistical error is essentially negligible compared to the systematic effects. Note that the consequences of violation of rotational symmetry are much less severe than in the gluon case, although they are still the dominant source of systematic errors. As the ghost is a scalar, this was somehow expected. Also, the finite-physical-volume errors are somewhat smaller than in the gluon case. Comparing the lattice data to the perturbative predictions [8] at the largest momentum (for $\beta = 6.0$) we find that the former are larger by about 6% and 5.5% for the lattice volumes $V = 20^3$ and $V = 30^3$, respectively. In this case, perturbation theory only deviates about 1% from the asymptotic tree-level value at this momentum. If one con-

[1] In the general case one considers $p \neq q$. However, in the case of the ghost propagator, one has $p = -q$ due to momentum conservation. Note that, again, we do not divide by the lattice volume V when considering the Fourier transform.

[2] When considering the plane-wave source the ghost propagator is the expectation value of a positive operator on the plane-wave state, i.e. the result is always positive-definite. This is not true with the point-source method. Indeed, one can obtain (on a given lattice configuration) a negative value for the quantity $(M^{-1})^{ab}(p)$. Nevertheless, on average, the ghost propagator $D_G(p)$ is positive for all values of the momentum p also when using the point-source method.

[3] In the present case, due to memory restrictions, we only consider subsequences of the CG iteration of length 1.

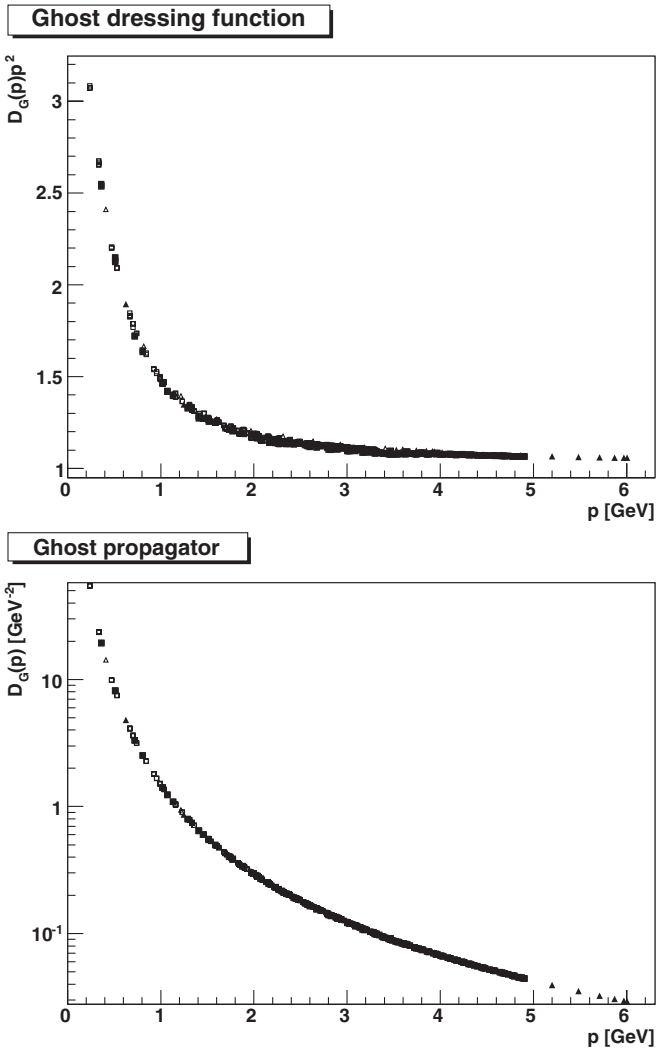

FIG. 2. The color-averaged diagonal part of the ghost dressing function $D_G(p)p^2$ (top) and of the ghost propagator $D_G(p)$ (in GeV^{-2}, bottom) as a function of the momentum p (in GeV). Open and full symbols are used for $\beta = 4.2$ and $\beta = 6.0$, respectively. In both cases we consider the lattice volume $V = 30^3$. Squares and triangles correspond to plane and diagonal momentum configurations, respectively.

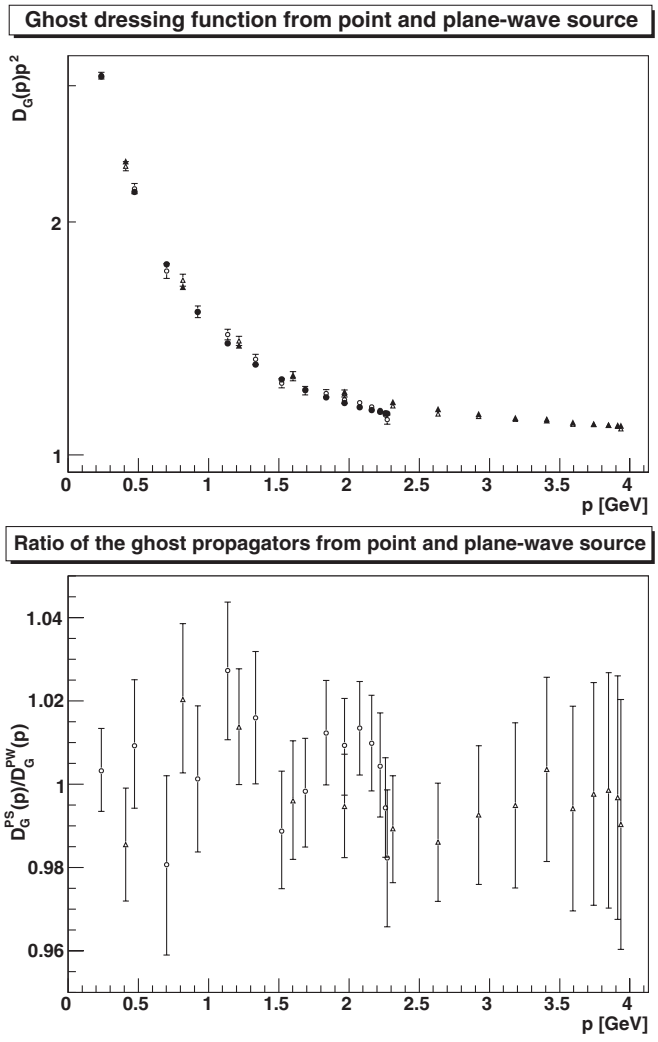

FIG. 3. In the top panel we show the ghost dressing function $D_G(p)p^2$ obtained using the plane-wave source (full symbols) and the point source (empty symbols) for $V = 30^3$ and $\beta = 4.2$. Note the logarithmic scale on the y axis. In the bottom panel we report the ratio of the point-source data (PS) with the plane-wave-source results (PW) for the ghost propagator. In both panels, circles denote momenta of type $(0, 0, p)$, triangles indicate diagonal momenta and the quantities are considered as a function of the momentum p (in GeV). Here, for both methods, we considered 380 configurations.

siders tadpole improvement [15], then the ghost propagator gets multiplied by u_0, i.e. by 0.92807 at $\beta = 4.2$ and by 0.95298 at $\beta = 6.0$, leading to a better agreement with perturbation theory.

Here we did not try to fit the data for the ghost propagator and obtain an estimate for its infrared exponent. Nevertheless, from Fig. 2 one clearly sees that $D_G(p)$ is more singular than $1/p^2$.

We also compared the results obtained using the two different inversion methods mentioned above (i.e. point-source and plane-wave-source methods). In the second case the inversion has been done using a CG method with even-odd preconditioning and a convergence test given by $|r|^2/|r_0|^2 \leq 10^{-8}$, where r and r_0 are the final and the initial residuals, respectively. The use of the even-odd preconditioning usually reduces the number of CG iterations by about a factor 2. We find that the results from these two methods agree on the average for the ghost propagator as well as for the ghost-gluon vertex, discussed below. As can be seen in Fig. 3, the ghost propagator obtained using the point source oscillates around the (smoother) result obtained using the plane-wave source. This oscillatory behavior is stronger for the ghost-gluon vertex, but vanishes in both cases when the statistics is increased, albeit much more slowly for the latter case.

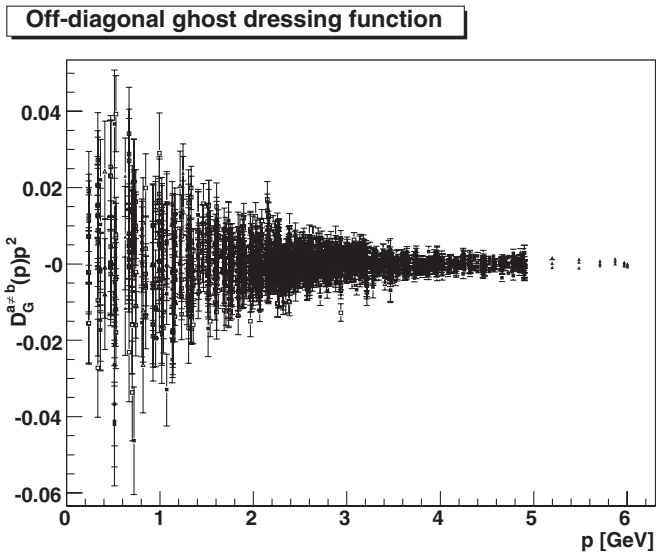

FIG. 4. The real part of the color upper-triangular matrix elements of the ghost dressing function $D_G^{ab}(p)p^2$ as a function of the momentum p (in GeV). Open and full symbols indicate $\beta = 4.2$ and $\beta = 6.0$, respectively. In both cases we consider the lattice volume $V = 30^3$. Squares and triangles correspond to plane and diagonal momentum configurations, respectively.

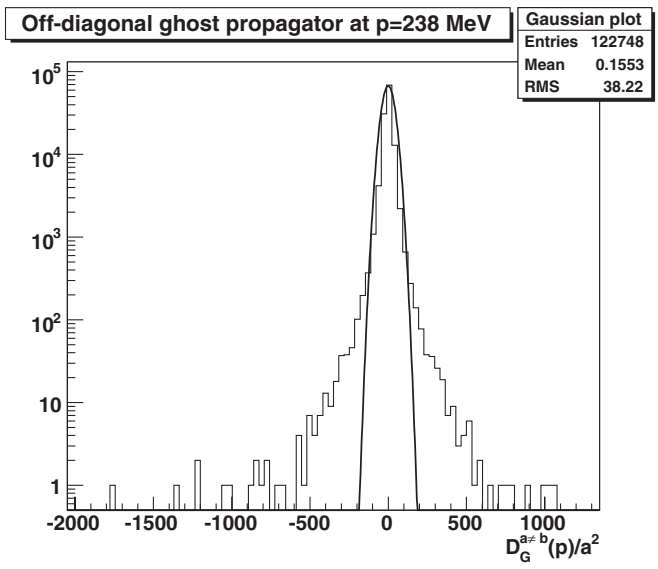

FIG. 5. A histogram of the real part of the off-diagonal elements of the ghost propagator (in lattice units) evaluated at the smallest momentum for the lattice volume $V = 30^3$ at $\beta = 4.2$. We also plot a Gaussian with the same mean and standard deviation as the histogram of the data.

An important assumption in functional calculations is that the ghost propagator is color diagonal.[4] In Fig. 4 we show results for the real part of the off-diagonal components of the ghost propagator.[5] The majority of the points are compatible with a null result, within the 67%-confidence interval, and the mean value of the (real part of the) off-diagonal propagator decreases for all momenta with increasing statistics. On the other hand, these fluctuations exhibit significantly enhanced tails (see Fig. 5). We checked that these large fluctuations are in most cases related to large values of the color-diagonal part of the ghost propagator and to configurations for which gauge fixing to Landau gauge required many more iterations than in the average case. Thus, these tails could be related to the exceptional configurations observed in [16]. Let us note that, by using the point-source method [46] for the inversion, one needs very large statistics in order to see a null average for the off-diagonal points in the infrared. Also, using this method, the real (respectively, imaginary) part of the inverse Faddeev-Popov matrix $(M^{-1})^{ab}(p, -p)$ is symmetric (respectively antisymmetric) only on average and not for each lattice configuration, as is the case when using the plane-wave source [49].

C. Eigenvalue spectrum of the Faddeev-Popov operator

The CG method has a close relationship with the so-called Lanczos algorithm, which can be used to extract the eigenvalues of a matrix [48]. As a consequence, it is possible to determine the ghost propagator and simultaneously obtain information on the eigenvalue spectrum. Note that only the *exact* CG algorithm is guaranteed to obtain the correct spectrum (up to degeneracy) of the Faddeev-Popov matrix after at most $(N_c^2 - 1)V$ inversion steps. On the other hand, working in finite-precision arithmetic (see Sec. 4 in [48]), the algorithm typically does not deliver a sufficiently accurate numerical approximation to all eigenvalues of this matrix. Indeed, as the number of iterations increases, the method has the property that the extremal eigenvalues evaluated are progressively improved approximations of the extremal eigenvalues of the matrix considered [51]. At the same time, since the procedure is stopped before all eigenvalues are found, the middle of the spectrum is usually not reliable and underpopulated. Moreover, each eigenvalue will be found only once, independently of its degeneracy. Still, when averaging over many configurations—i.e. when considering a histogram of the eigenvalues found for all the configurations, normalized by the total number of eigenvalues[6]—one should be

[4]We also checked that the real part of the color-off-diagonal components of the gluon propagator is essentially zero within statistical errors and that its central value decreases with increasing statistics. Of course, the imaginary part vanishes identically.

[5]Let us recall that the fluctuations of the *imaginary* part of the off-diagonal elements of the ghost propagator are connected to the possible existence of a ghost condensate [49]. In particular, non-Gaussian fluctuations could indicate the existence of a spontaneous-symmetry breaking and a nonvanishing value for this condensate. (For a different interpretation, see Ref. [50].) In this work we do not present data for the ghost condensate.

[6]Doing this normalization for each inversion and each configuration separately does not yield a different result within the statistical errors.

able to obtain an idea of the density of the eigenvalues at both ends of the spectrum. In particular, one can verify whether the shape of the eigenvalue density (at small eigenvalues) is flat or increases with the magnitude of the eigenvalues ω, thus gaining information on the validity of the Gribov-Zwanziger scenario. On the other hand, the upper end of the spectrum, which is also obtained, is essentially determined by perturbative contributions and thus not as interesting.

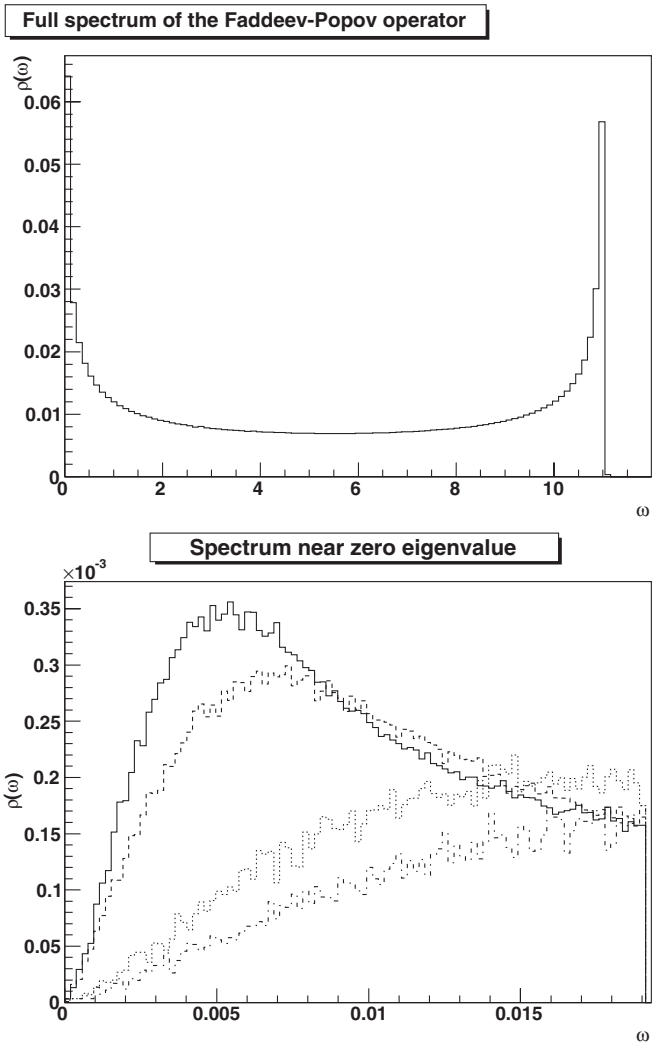

FIG. 6. The density $\rho(\omega)$ of the eigenvalues of the Faddeev-Popov operator (using the Lanczos method) as a function of their magnitude ω (in lattice units), normalized by the total number of eigenvalues. In the top panel we show the complete results while in the bottom panel only the density for small eigenvalues is presented. In both cases we considered 100 bins (this explains the different scale on the y axis). The solid line (in both panels) refers to the lattice volume $V = 30^3$ at $\beta = 4.2$. In the bottom panel, the dashed line correspond to $V = 30^3$ at $\beta = 6.0$, the dotted line to $V = 20^3$ at $\beta = 4.2$ and the dashed-dotted line to $V = 20^3$ at $\beta = 6.0$. The total number of eigenvalues determined are 4 374 822 ($V = 20^3$, $\beta = 4.2$), 11 312 874 ($V = 30^3$, $\beta = 4.2$), 3 549 202 ($V = 20^3$, $\beta = 6.0$) and 9 862 721 ($V = 30^3$, $\beta = 6.0$).

The results are shown in Fig. 6 (top panel). The full spectrum is shown for completeness. As said above, the small density of the spectrum for intermediate magnitude ω of the eigenvalues is very likely an artifact of the algorithm. For very small magnitude ω (see Fig. 6, bottom panel) the spectrum shows a linear increase with ω. The steepness is much larger on the larger lattices and it also seems to increase with the physical volume, i.e. as β decreases. These results are in qualitative agreement with those reported in Ref. [32] for the four-dimensional case. Note, however, that a linear increase at small momenta is different from the result obtained in Coulomb gauge in four dimensions [52], where a powerlike behavior has been observed.

Using a preconditioned CG method we have also evaluated the smallest and the largest eigenvalues of the Faddeev-Popov matrix M. Results are reported in Table III. For comparison we also give the smallest and the largest eigenvalues of the lattice Laplacian $-\Delta$ for the same lattice size. Let us recall that in d dimensions, the smallest eigenvalue of $-\Delta$ is given by $4\sin^2(\pi/2N)$, while the largest is equal to $4d\sin^2[\pi(N-1)/2N]$. We see that the largest eigenvalue of M depends weakly on the lattice volume V and on the coupling β. On the other hand, for a given β, the smallest eigenvalue decreases faster than the corresponding eigenvalue of $-\Delta$, as the lattice side increases. This is in agreement with the results reported in [47]. Also, if we consider the smallest eigenvalue of M in physical units, i.e. if we multiply it by $1/a^2$, we find the results reported in Fig. 7. If one tries a fit to data using the Ansatz a/L^c we obtain that the data are well fitted for $c = 2.62(8)$ (with $\chi/\text{d.o.f.} = 1.4$). This seems to suggest that for these lattice volumes and β values we are in the scaling region for ω_s and that this eigenvalue goes to zero when the infinite-volume limit is approached. As a consequence, in the continuum limit, the average lattice Landau configuration should belong to the first Gribov horizon, supporting the Gribov-Zwanziger mechanism of confinement.

TABLE III. Largest and smallest eigenvalues of the Faddeev-Popov matrix (respectively, ω_l and ω_s, both in lattice units) for each lattice volume V and coupling β. We also report the corresponding eigenvalues of the lattice Laplacian (for the same lattice side N). For the lattice volume $V = 20^3$ we consider 200 configurations at $\beta = 4.2$ and 400 at $\beta = 6.0$; for $V = 30^3$ we have 380 and 500 configurations at $\beta = 4.2$ and 6.0, respectively.

Volume	β	ω_l	ω_s	$\omega_{l,\text{Lapl.}}$	$\omega_{s,\text{Lapl.}}$
20^3	4.2	11.1218(9)	0.0072(2)	11.9261	0.0246
30^3	4.2	11.1337(5)	0.00275(6)	11.9671	0.0110
20^3	6.0	11.4050(4)	0.0102(2)	11.9261	0.0246
30^3	6.0	11.4149(2)	0.00353(7)	11.9671	0.0110

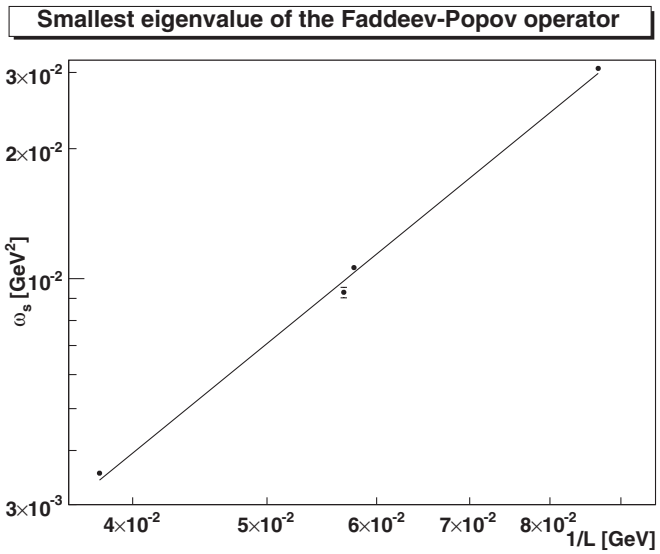

FIG. 7. Plot of the smallest eigenvalue ω_s (in GeV^2) of the Faddeev-Popov matrix, as a function of the inverse lattice side $1/L$ (in GeV), and of the fitting function a/L^c with $a = 18.127$ and $c = 2.6152$.

IV. VERTICES

In Yang-Mills theory (without valence and sea quarks) there are two nonvanishing 3-point Green's functions: the three-gluon vertex and the ghost-gluon vertex. Compared to the propagators, these are quite complicated since there are now three kinematical variables. In addition, for the three-gluon vertex there exist a large number of tensor structures [53]. Therefore, it is impractical to investigate all tensor structures for all possible kinematical configurations. Furthermore, due to kinematics, the interesting signal—i.e. an appropriately defined dimensionless function—is usually suppressed at large momenta as $1/p^6$ instead of as $1/p^2$ (except for some particular momentum configurations for which it is only suppressed by $1/p^4$). Thus, it is in general quite difficult to obtain a good signal/noise ratio at large p.

Let us recall that, due to momentum conservation, the three momenta of the vertices always lie in one plane and are completely characterized by the size of two of the momenta and by the angle ϕ between them. Two particular momentum configurations are of special importance. In the first case two of the momenta are orthogonal with respect to each other (this configuration will be called here the *orthogonal* one). This configuration enters into loop integrals with maximum angular weight[7] and, as we will see below, has the advantage of relatively small statistical fluctuations. In this case we take the two orthogonal momenta, respectively, along the x and y axis, considering all possible magnitudes of both momenta independently. If one of these two momenta vanishes, then one recovers the kinematical configuration used in several previous lattice studies of these vertices [25,29–31].

In the second configuration (called here the *equal* one) the three momenta have the same magnitude and the angle ϕ is equal to $\pi/3$. The vertex is then a function of only one variable. For this configuration the infrared behavior of the n-point Green's functions can be taken to be the limit where all n momenta vanish in the same way, i.e. only one scale has to be considered. In this case there are predictions for the behavior of the n-point Green's functions in the infrared limit, from studies using Dyson-Schwinger equations (DSEs) [10,11]. Of course, on the lattice, it is not possible (in general) to select three equal momenta, for example, in the $x - y$ plane. However, one can consider the momenta $(p, -p, 0)$, $(-p, 0, p)$ and $(0, p, -p)$, which all have the (lattice) size $\sqrt{2}P$ with $P = 2\sin(\pi p/N)$.

Let us recall that, due to the invariance of the lattice theory under hyper-cubic transformations, the results should be invariant by reflection of the momenta. This implies that—with the exception of $p = 0$ and of the midpoint on even lattices—we can average over two different kinematical configurations for each physical momentum. For the vertices, due to momentum conservation, we can apply the reflection transformation only to the independent momenta. In particular, in the orthogonal case, we can apply the reflection independently on the two orthogonal momenta, i.e.—for each physical momentum configuration—we can average over four different kinematical configurations. On the contrary, in the equal-momenta case, the reflection has to be applied at the same time on the three momenta, i.e. each time we can average over two different kinematical configurations. Let us note that this averaging allows us to cancel exactly, on each lattice configuration, contributions that would otherwise be zero only on average, yielding purely imaginary vertices.

Finally, one has to consider the tensor structure of the vertices, which is not straightforward for the three-gluon vertex. In functional-method studies it is particularly interesting to know how different a vertex is from its tree-level structure. Thus, we consider here the projection of the vertices on their tree-level values, obtaining a scalar function normalized to 1 when the tree-level vertex and the full vertex are equal.

A. Three-gluon vertex

The three-gluon vertex $\Gamma^{\mathrm{tl},A^3,abc}_{\mu\nu\rho}(p, q, k)$ (with $k = -p - q$) at tree-level in the continuum has the form

$$\Gamma^{\mathrm{tl},A^3,abc}_{\mu\nu\rho}(p, q, k) = -igf^{abc}[(q - k)_\mu \delta_{\nu\rho} + (k - p)_\nu \delta_{\mu\rho} + (p - q)_\rho \delta_{\mu\nu}], \quad (14)$$

while on the lattice one finds [41]

[7] Let us recall that this angular weight is proportional to $\sin(\phi)$ in 3d.

$$\Gamma^{\mathrm{tl},L,A^3,abc}_{\mu\nu\rho}(p,q,k) = -igf^{abc}e^{i\pi(p_\mu+q_\nu+k_\rho)/N}[(\widetilde{q-k})_\mu \times \delta_{\nu\rho}\cos(\hat{p}_\nu) + (\widetilde{k-p})_\nu\delta_{\mu\rho}\cos(\hat{q}_\rho) + (\widetilde{p-q})_\rho\delta_{\mu\nu}\cos(\hat{k}_\mu)]. \quad (15)$$

Note that the cosine factors in the above equation go to 1 in the formal continuum limit $a \to 0$, for a fixed physical lattice side $L = Na$. The same applies to the exponential prefactor. Here we used the notation

$$\tilde{p}_\mu = 2\sin(\hat{p}_\mu) \equiv P_\mu \quad (16)$$

$$\hat{p}_\mu = \frac{\pi p_\mu}{N} \quad (17)$$

with p_μ taking values $0, \ldots, N/2$. Clearly, the three-gluon vertex is totally symmetric under the simultaneous exchange of color index, Lorentz index and momentum, and thus completely Bose-symmetric.

The full three-gluon vertex $\Gamma^{A^3,abc}_{\mu\nu\rho}$ is not directly available on the lattice, but one can evaluate the corresponding full Green's function [29]

$$G^{A^3,abc}_{\mu\nu\rho}(p,q,k) = \frac{1}{V}\langle A^a_\mu(p)A^b_\nu(q)A^c_\rho(k)\rangle. \quad (18)$$

As said above, momentum conservation requires $k = -p - q$. Because of the vanishing of any vector condensates in Yang-Mills theory, this Green's function equals the connected Green's function, but it is still necessary to amputate it. The relation of the full vertex $\Gamma^{A^3,\mathrm{def}}_{\lambda\sigma\omega}(p,q,k)$ with the Green's function is then given by

$$G^{A^3,abc}_{\mu\nu\rho}(p,q,k) = D^{ad}_{\mu\lambda}(p)D^{be}_{\nu\sigma}(q)D^{cf}_{\rho\omega}(k)\Gamma^{A^3,def}_{\lambda\sigma\omega}(p,q,k). \quad (19)$$

In Landau gauge, one can extract only the transverse part of the full vertex. In order to project the quantity above on the tree-level vertex, the following function will be evaluated

$$G^{A^3}(p,q,\phi) = \frac{\Gamma^{\mathrm{tl},L,A^3,abc}_{\mu\nu\rho}(p,q,k)G^{A^3,abc}_{\mu\nu\rho}(p,q,k)}{\Gamma^{\mathrm{tl},L,A^3,abc}_{\mu\nu\rho}(p,q,k)D^{ad}_{\mu\lambda}(p)D^{be}_{\nu\sigma}(q)D^{cf}_{\rho\omega}(k)\Gamma^{\mathrm{tl},L,A^3,\mathrm{def}}_{\lambda\sigma\omega}(p,q,k)} \quad (20)$$

$$= \frac{\Gamma^{\mathrm{tl},L,A^3,abc}_{\mu\nu\rho}(p,q,k)G^{A^3,abc}_{\mu\nu\rho}(p,q,k)}{\Gamma^{\mathrm{tl},L,A^3,abc}_{\mu\nu\rho}(p,q,k)P_{\mu\lambda}(p)P_{\nu\sigma}(q)P_{\rho\omega}(k)\Gamma^{\mathrm{tl},L,A^3,abc}_{\lambda\sigma\omega}(p,q,k)D(p)D(q)D(k)}, \quad (21)$$

where the D's are the scalar gluon propagators. Clearly, this function is equal to 1 if the full vertex is equal to the bare vertex. Note that, by contracting the Green's function with the lattice version of the tree-level vertex instead of the continuum version corrects for (relevant) discretization effects. Also note that the exponential prefactor in Eq. (5) implies a prefactor $\exp[-i\pi(p_\mu + p_\lambda)/N]$ for the gluon propagator $D^{ad}_{\mu\lambda}(p)$. Thus, considering Eq. (15), all these prefactors cancel each other both in the numerator and in the denominator of Eq. (20) above.

The normalization factor in the denominator is in some kinematical cases quite simple, but in general very lengthy and will not be given here explicitly. Also, this normalization factor vanishes for the largest momentum in each momentum configuration due to the cosine factors. Thus, this momentum cannot be considered. The same applies to the case where all momenta vanish.

Let us stress that, although the quantity in Eq. (21) is 1 if the full and the tree-level vertex coincide, it will in general have contributions from tensor structures not appearing at the tree level. The situation would be even more complicated in the case of a vertex not totally antisymmetric in color space. In the continuum, the general tensor structure of the total color-antisymmetric part of the full three-gluon vertex is given by [53]

$$\Gamma^{A^3,abc}_{\mu\nu\rho}(p,q,k) = -if^{abc}\Big(A(p,q,k)\delta_{\mu\nu}(p_\rho - q_\rho) + B(p,q,k)\delta_{\mu\nu}(p_\rho + q_\rho) + C(p,q,k) \times (p_\nu q_\mu - \delta_{\mu\nu}p\cdot q)(p_\rho - q_\rho) + \frac{S(p,q,k)}{3}(p_\rho q_\mu k_\nu + p_\nu q_\rho k_\mu)\Big) + \text{cyc.perm.}, \quad (22)$$

where A, B, C and S are scalar functions. (See again Ref. [53] for the symmetry properties of these functions.) Then, one can verify that, in the continuum, the quantity (21) contains only contributions from the functions A and C. For example, in the orthogonal configuration, using the above equation one finds

$$G^{A^3c}\left(p,q,\frac{\pi}{2}\right) = \{xyA(p,q,k) + (x+y)[2yA(k,p,q) + 2xA(q,k,p) + (xy+2y^2)C(k,p,q) + (2x^2+xy)C(k,q,p) + xyC(q,p,k)]\}/(2x^2+5xy+2y^2), \quad (23)$$

where $x = q^2$ and $y = p^2$. The expression is lengthier for other kinematical configurations.

It then only remains to determine the 3-point Green's function. This can be done in a straightforward way using the definition (18) and the Fourier-transformed gauge fields defined in Eq. (5). The only problem is that the functions $A^a_\mu(p)$ vanish on average. This induces very large fluctuations in the calculation of the Green's function, particularly at large momenta. This problem makes the extraction of the equal-momentum configuration quite complicated. In the orthogonal configuration the situation is slightly better, since some field components identically vanish even for nonvanishing momenta, as discussed in Sec. III, reducing the statistical noise. Also note that, in the evaluation of Eq. (21), the Green's function and the propagators are calculated independently and divided after averaging over all lattice configurations. The error can then be determined by error propagation, but due to the smallness of the statistical errors on the propagators, their errors are neglected here.

Let us note that, from the discussion in Sec. III A, we found that (with our notation) the continuum momentum-space gluon field has mass dimension $-1 - d/2$ while the gluon propagator, again in momentum space, has mass dimension -2. This implies that the full Green's function defined in Eq. (18) has mass dimension $-3 - d/2$. The same result can be obtained by considering Eq. (19) after observing that the three-gluon vertex $\Gamma^{A^3,\mathrm{def}}_{\lambda\sigma\omega}(p, q, k)$ has mass dimension $3 - d/2$ [see also the tree-level result in Eq. (14)]. Thus, the quantity considered in Eq. (20) is inherently dimensionless and we do not have to multiply it by any power of the lattice spacing a. On the other hand, in order to get the corresponding continuum quantities we have to multiply the momentum-space lattice gluon field and the gluon propagator by $\sqrt{\beta}$ and by β, respectively. It follows that the scalar function $G^{A^3}(p, q, \phi)$ has to be divided by $\beta^{3/2}$ in order to obtain the corresponding continuum quantity.

Three different momentum configurations are shown in Fig. 8. The first is the momentum configuration used in [25,29–31] to study the behavior of the strong-coupling constant. Note that this configuration is not well-defined in the continuum limit in case the Gribov-Zwanziger scenario is correct, i.e. if the gluon propagator vanishes at zero momentum. Of course, on a finite lattice this is not a problem. In the second case, two momenta are equal and orthogonal. Finally, the third case corresponds to three momenta with the same magnitude. Furthermore, the behavior of $G^{A^3}(p, q, \phi)$ as a function of p and q is shown in Fig. 9.

As said above, the statistical errors are quite large at large momenta, even after averaging over more than 20 000 configurations. Let us recall that, in some cases, the data shown in Fig. 8 have been obtained by summing more than 700 different terms. In particular we checked that, at large

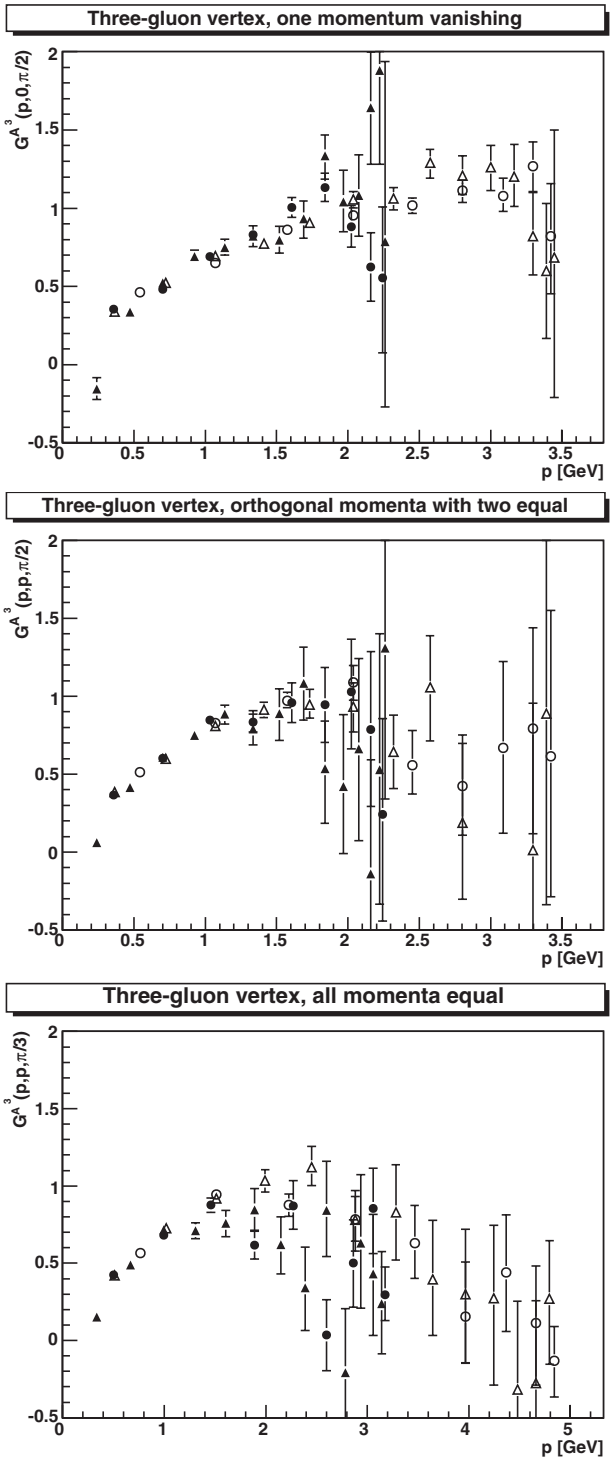

FIG. 8. The scalar function $G^{A^3c}(p, q, \phi)$ defined in Eq. (20). Full symbols correspond to $\beta = 4.2$ and open symbols to $\beta = 6.0$; circles are used for $V = 20^3$ and triangles for $V = 30^3$. In the top panel we show results for the orthogonal configuration with one momentum (q) vanishing. In the middle panel we consider an orthogonal configuration with two momenta having the same magnitude ($p = q$). In the bottom panel we plot data for the case with the three momenta equal ($p = q = k$).

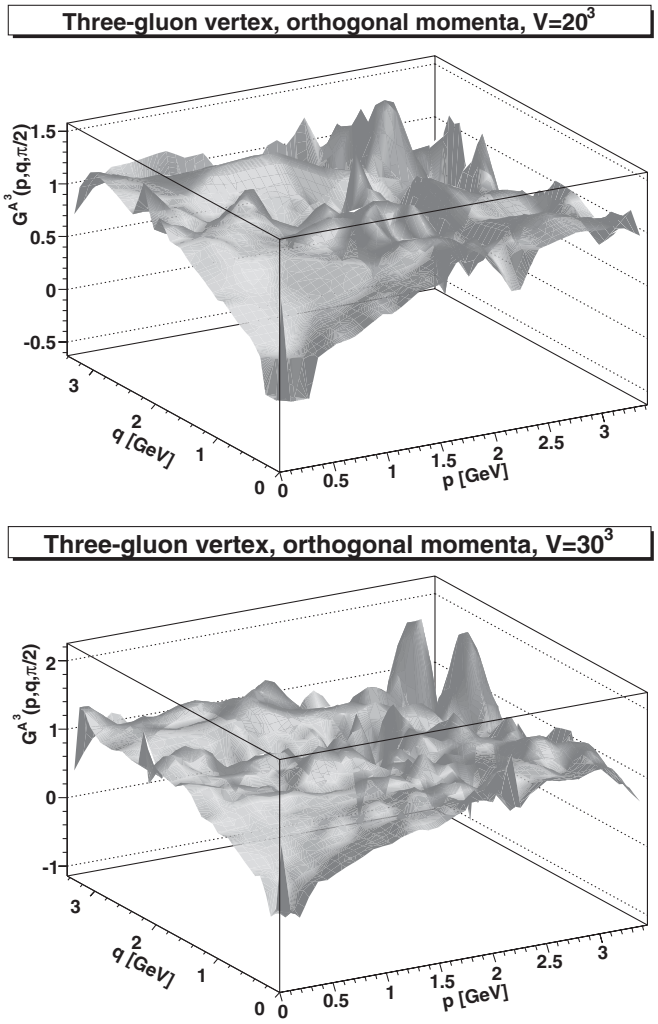

FIG. 9. The scalar function $G^{A^3c}(p, q, \phi)$ defined in Eq. (20) as a function of the magnitude of the gluon momenta p and q (for the orthogonal configuration). Here, for each data point, we plot only the central value. The data for $\beta = 4.2$ and $\beta = 6.0$ are plotted together and they are interpolated by Gouraud shading, as implemented in the ROOT package [56]. In the top figure we used data for the lattice volume $V = 20^3$; in the bottom one we consider the lattice volume $V = 30^3$. Spikes indicate positions where due to fluctuations the value is outside the drawing range. The spike at $p = q = 0$ is an artifact since this quantity cannot be evaluated when the three momenta are null.

p, the central values of the data can change substantially if one considers different subsets of the whole set of configurations used in the analysis. This suggests that the statistical error obtained at large p is likely underestimated.

Despite the large statistical fluctuations at large momenta, the vertex clearly decreases in the limit of small momenta. This behavior can be observed in the three plots in Fig. 8 and also in Fig. 9, for all directions approaching the limit $p = q = k = 0$. On the other hand, at the smallest momentum point on the 30^3 lattice at $\beta = 4.2$ (see top panel in Fig. 8), i.e. for the orthogonal configuration, the vertex is clearly negative. Of course, with our data we cannot say if the vertex would stay finite or would become larger (in absolute value) as the zero momentum limit is approached. Indeed, we know that, with our lattice volumes and β values, the true infrared regime is not reached yet, since the gluon propagator is not suppressed at small momenta [18]. Clearly, if the 3-point Green's function stays constant in the infrared limit, while the propagators get suppressed, the vertex $\Gamma^{A^3,abc}_{\mu\nu\rho}(p, q, \phi)$ may be enhanced, as predicted by studies using functional methods in four dimensions [10] and in three dimensions [11].

Finally, in order to test whether other tensor structures are relevant, the vertex has also been contracted with itself instead of using the tree-level vertex. Results are not presented here, but we find that the corresponding scalar function shows a strong increase compared to the tree-level behavior at large momenta. This suggests that other tensor structures also contribute to the vertex in a nontrivial way.

B. Ghost-gluon vertex

The ghost-gluon vertex can be treated essentially along the same lines as the three-gluon vertex. Let us recall that at the tree level, in the continuum, this vertex is given by

$$\Gamma^{\mathrm{tl},c\bar{c}A,abc}_{\mu}(p, q, k) = igf^{abc}q_{\mu}, \tag{24}$$

while on the lattice one finds [41]

$$\Gamma^{\mathrm{tl},L,c\bar{c}A,abc}_{\mu}(p, q, k) = igf^{abc}e^{i\pi k_{\mu}/N}\tilde{q}_{\mu}\cos(\hat{q}_{\mu}). \tag{25}$$

Again, the cosine and the exponential are lattice artifacts, going to 1 in the formal continuum limit $a \to 0$. Also, on the lattice it is only possible to determine the full Green's function

$$G^{c\bar{c}A,abc}_{\mu}(p, q, k) = \frac{1}{V}\langle c^a(p)\bar{c}^b(q)A^c_{\mu}(k)\rangle, \tag{26}$$

where c^a (respectively $\bar{c}^b$) is the ghost (respectively antighost) field. Then, the scalar quantity we evaluate is defined by

$$G^{c\bar{c}A}(q, k, \phi) = \frac{\Gamma^{\mathrm{tl},L,c\bar{c}A,abc}_{\mu}(p, q, k)G^{c\bar{c}A,abc}_{\mu}(p, q, k)}{\Gamma^{\mathrm{tl},L,c\bar{c}A,abc}_{\mu}(p, q, k)D^{ad}_{G}(p)D^{be}_{G}(q)D^{cf}_{\mu\nu}(k)\Gamma^{\mathrm{tl},L,c\bar{c}A,def}_{\nu}(p, q, k)} \tag{27}$$

$$= \frac{\Gamma^{\mathrm{tl},L,c\bar{c}A,abc}_{\mu}(p, q, k)G^{c\bar{c}A,abc}_{\mu}(p, q, k)}{\Gamma^{\mathrm{tl},L,c\bar{c}A,abc}_{\mu}(p, q, k)P_{\mu\nu}(k)\Gamma^{\mathrm{tl},L,c\bar{c}A,abc}_{\nu}(p, q, k)D_{G}(p)D_{G}(q)D(k)} \tag{28}$$

$$= \frac{-igf^{abc}\tilde{q}_\mu \cos(\hat{q}_\mu) G^{c\bar{c}A,abc}_\mu(p,q,k)}{g^2 N_c (N_c^2-1)\tilde{q}_\mu \cos(\hat{q}_\mu) P_{\mu\nu}(k)\tilde{q}_\nu \cos(\hat{q}_\nu) D_G(p) D_G(q) D(k)}, \tag{29}$$

where D_G is the ghost propagator and we used Eq. (25). Note that we have neglected in the denominator the color off-diagonal components of the propagators and used the relation $f^{abc}f^{abc} = N_c(N_c^2-1)$. Also, due to the implicit contraction of the full Green's function with a gluon propagator, only one tensor structure survives, which is proportional to the incoming antighost momentum q. Finally, as for the three-gluon vertex, the exponential prefactors cancel out in the numerator and in the denominator of the scalar function defined above.

For the ghost-gluon vertex, the normalization factors are quite simple and will be given explicitly. In the orthogonal case, we considered a gluon momentum k aligned along the y-axis, while the incoming antighost momenta q is chosen along the x-axis. This implies $q_\mu P_{\mu\nu}(k) = q_\nu$. Thus, the denominator in Eq. (29) is proportional to

$$\sum_\mu \tilde{q}_\mu^2 \cos^2(\hat{q}_\mu) = \tilde{q}_x^2 \cos^2(\hat{q}_x), \tag{30}$$

where the last equality follows because the momentum q is aligned along the x-direction. Clearly, in this case one recovers the kinematical normalization considered in Ref. [25]. In the case of equal momenta, the situation is more complicated and an explicit Gram determinant appears. Indeed, by choosing the gluon momentum k in the $x-y$ plane and the incoming antighost momentum q in the $x-z$ plane, the denominator is proportional to

$$\tilde{q}_x^2 \cos^2(\hat{q}_x)\left(1 - \frac{\tilde{k}_x^2}{\tilde{k}_x^2 + \tilde{k}_y^2}\right) + \cos^2(\hat{q}_z)\tilde{q}_z^2. \tag{31}$$

In the case of equal components $|\hat{q}_x| = |\hat{q}_z| = |\hat{k}_x| = |\hat{k}_y| = |\hat{q}|$ this expression simplifies to $3\tilde{q}^2\cos^2(\hat{q})/2$. Note that, in both cases, the normalization would be the same in the four-dimensional case, since all momenta considered are in a three-dimensional subspace. Finally, it should be noted that the only Lorentz indices of $G^{c\bar{c}A,abc}_\mu(p,q,k)$ contributing to the numerator are those corresponding to nonzero components of the incoming antighost momentum q. Thus, in the orthogonal configuration the argument of the exponential prefactor appearing in Eq. (5) is always zero for the Lorentz components contributing to $G^{c\bar{c}A,abc}_\mu(p,q,k)$.

Let us also note that, when contracted with the transverse projector $P_{\mu\nu}(k)$ of the gluon momentum k (as done here), the vertex should be invariant under the exchange of the ghost and of the antighost fields [24]. This is of course true at the tree-level [see Eq. (24)], since it corresponds to an exchange of the color indices a and b and to replacing q by $p = -k - q$. Indeed, the term proportional to k_μ vanishes, due to the contraction with $P_{\mu\nu}(k)$, and the minus sign of $-q_\mu$ cancels with the minus sign related to the antisymmetry of the structure constant. In the general case this invariance is a consequence of a global $SL(2,R)$ symmetry between ghosts and antighosts (see Appendix A in Ref. [6] for a proof of this symmetry in Landau gauge). As the Green's function (33) is implicitly contracted with a gluon propagator, it follows that

$$G^{c\bar{c}A,abc}_\mu(p,q,k) = G^{c\bar{c}A,bac}_\mu(q,p,k). \tag{32}$$

This result is also related to the symmetry of the Faddeev-Popov matrix under simultaneous exchange of space and color indices.

The only remaining task is then to determine the quantity defined in Eq. (26) above. Since on the lattice one does not consider ghost (and antighost) fields, the (equivalent) expression to be used is [25]

$$G^{c\bar{c}A,abc}_\mu(p,q,k) = \frac{1}{V}\langle (M^{-1})^{ab}(p,q) A^c_\mu(k)\rangle. \tag{33}$$

One can employ the point-source method, used for evaluating the ghost propagator, also in the case of the ghost-gluon-vertex function. Indeed, by using translational invariance we can write[8]

$$\langle M^{-1}(x,y)A(z)\rangle = \langle M^{-1}(0,y-x)A(z-x)\rangle. \tag{34}$$

Then, by using momentum conservation, i.e. $p = -k - q$, and the equation above we obtain

$$\begin{aligned}
&\frac{1}{V}\sum_{xyz} e^{2\pi i(-(k+q)x+qy+kz)/N}\langle M^{-1}(x,y)A(z)\rangle \\
&= \frac{1}{V}\sum_{xyz} e^{2\pi i[q(y-x)+k(z-x))]/N}\langle M^{-1}(0,y-x)A(z-x)\rangle \\
&= \sum_{yz} e^{2\pi i(qy+kz)/N}\langle M^{-1}(0,y)A(z)\rangle \\
&= \sum_{xyz} e^{2\pi i(qy+kz)/N}\langle M^{-1}(x,y)A(z)\delta_{x0}\rangle \\
&= \sum_{xyz} e^{2\pi i(qy+kz)/N}\langle M^{-1}(x,y)A(z)\left(\delta_{x0} - \frac{1}{V}\right)\rangle.
\end{aligned}$$

In the third line we have redefined the indices y and z and summed over x. In the last line we added a term that vanishes for nonvanishing ghost momenta [46]. Clearly, the quantity $\delta_{x0} - 1/V$ has a null value when summed over x, i.e. the inversion of the Faddeev-Popov operator is done in the subspace orthogonal to the (trivial) kernel of M. Thus, one can evaluate the Green's function by considering

[8]Here, in order to simplify the notation, we omit the color indices.

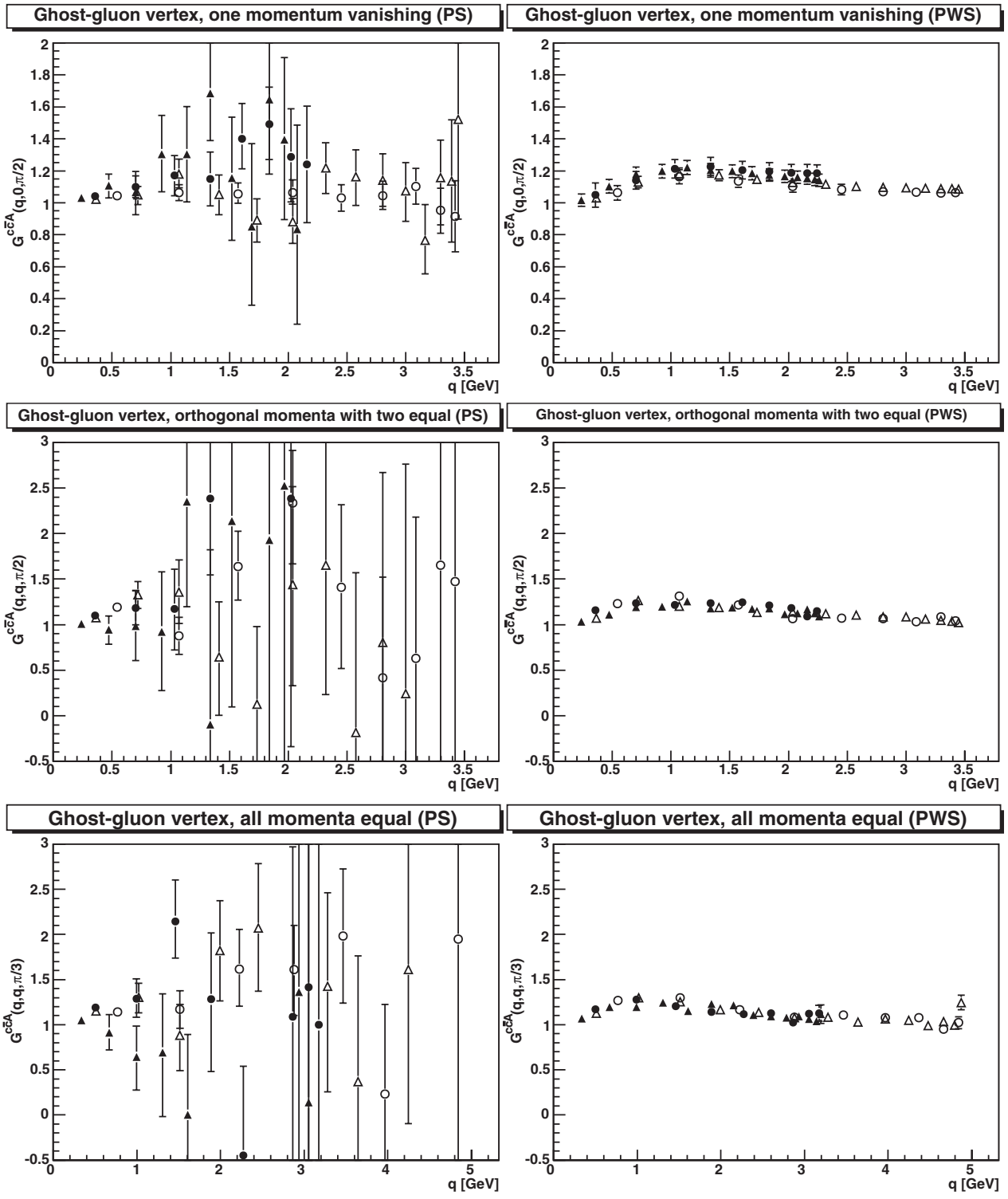

FIG. 10. The scalar quantity $G^{c\bar{c}A}(q, k, \phi)$ defined in Eq. (27) as a function of the magnitude of the incoming antighost momentum q. Full symbols correspond to $\beta = 4.2$ and open symbols to $\beta = 6.0$; circles are used for $V = 20^3$ and triangles for $V = 30^3$. Results on the left-hand side have been obtained using a point source (PS) while on the right-hand side we considered a plane-wave source (PWS). In the top panel we show results for the orthogonal configuration with the gluon momentum k vanishing. In the middle panel we consider an orthogonal configuration with the two momenta (q and k) having the same magnitude. In the bottom panel we plot data for the case with the three momenta equal. For the number of configurations considered in the PWS case, see caption of Table III.

the Fourier-transformed gluon field and by inverting the Faddeev-Popov operator using the point-source method. The final step requires one to evaluate the Fourier transform using the incoming antighost momenta q, i.e. the one appearing in the tree-level vertex. The third momentum (i.e. p) is implicitly defined by momentum conservation. As said above, the point-source method has the advantage of only $N_c^2 - 1$ inversions per configuration but, compared to the plane-wave-source method, requires many more configurations in order to achieve a given statistical accuracy.

Note that, since the momentum-space ghost propagator D_G has mass dimension -2, we have that the full Green's function $G_\mu^{c\bar{c}A,abc}(p, q, k)$ [see Eq. (33)] has mass dimension $-3 - d/2$. At the same time, the ghost-gluon vertex $\Gamma_\mu^{\mathrm{tl},L,c\bar{c}A,abc}(p, q, k)$ [see Eq. (24)] has mass dimension $3 - d/2$. Thus, also in this case the scalar function considered is clearly dimensionless and we do not have to multiply it by any power of the lattice spacing a. On the other hand, in order to get the corresponding continuum quantities we have to divide it by $\beta^{1/2}$.

Results are shown in Figs. 10 and 11. In the left column of Fig. 10 we show the results obtained using the point-source method, while on the right column we present the data obtained using the plane-wave source, for the vertex and for the ghost propagator appearing in Eq. (29). We see

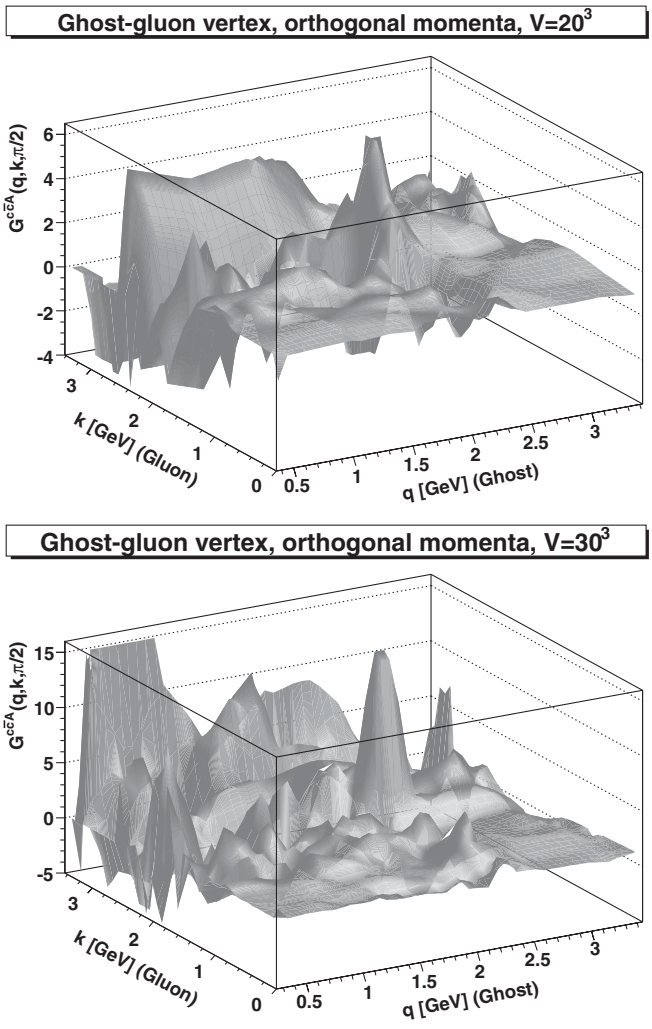

FIG. 11. The scalar quantity $G^{c\bar{c}A}(q, k, \phi)$ defined in Eq. (27) as a function of the magnitude of the incoming antighost momentum q and of the gluon momentum k (for the orthogonal configuration) using the point-source method. Here, for each data point, we plot only the central value. The data for $\beta = 4.2$ and $\beta = 6.0$ are plotted together and they are interpolated by Gouraud shading, as implemented in the ROOT package [56]. In the top figure we used data for the lattice volume $V = 20^3$; in the bottom one we consider the lattice volume $V = 30^3$. Spikes indicate positions where, due to fluctuations, the value is outside the drawing range. The large spikes below the smallest nonzero antighost momentum q are an artifact of the interpolation.

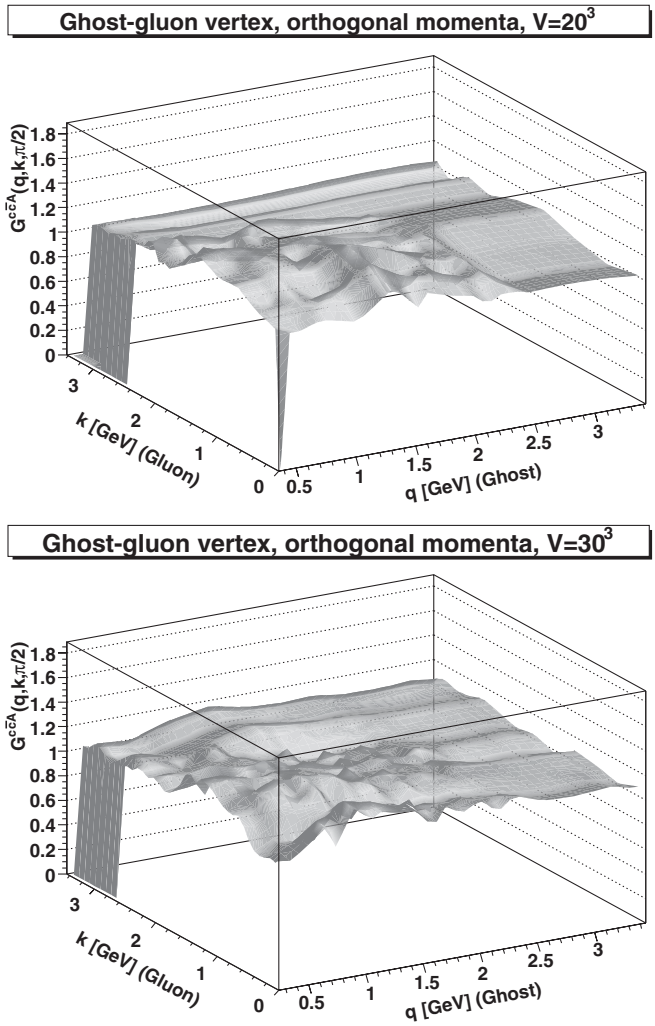

FIG. 12. Same as Fig. 11, but using a mixed point-source/plane-wave-source method. The number of configurations considered here are 283 and 269 for the lattice volume $V = 20^3$ at $\beta = 4.2$ and $\beta = 6.0$, respectively, and 227 and 213 configurations for $V = 30^3$ at $\beta = 4.2$ and $\beta = 6.0$.

agreement between the two sets of data but, as said above, the fluctuations are much smaller in the latter case, the relative error being of the order of 5% for all momenta. On the other hand, when considering the point-source method (left column) the fluctuations become rather large with increasing gluon momentum, i.e. the results rapidly lose accuracy. Let us finally note that the results on the right column do not change visibly if one evaluates the ghost propagator using the point-source method and the vertex using the plane-wave source (see Fig. 12).

Clearly, in all cases the vertex is essentially constant and of order one, for all momentum configurations, confirming the results obtained in the 4d case [25,26]. This would imply a fulfillment of the corresponding Slavnov-Taylor identity [54]. This result is also in very good agreement with the functional predictions in the 3d case [11,12] and the usual assumptions made in functional calculations.

V. SUMMARY AND OUTLOOK

In this work we have evaluated the three-point vertices of (pure) Yang-Mills theory using a wide range of momentum configurations. In order to reduce the computational cost we considered the 3d SU(2) case. We note that the data for the three-gluon vertex suffer from large statistical errors at large momenta, even when considering more than 20 000 configurations. Let us mention that, from a preliminary study [55], this problem seems to be less severe in the 4d case. For the ghost-gluon vertex the data also show a large ratio noise/signal if one uses the point-source method. In this case the use of the plane-wave source (for the vertex) allows to reduce the error below 10% already with a few tens of configurations.

As for the infrared behavior of the vertices, we found that the three-gluon vertex becomes very small as the momentum decreases. This midmomentum suppression is similar to the behavior considered for this vertex in Ref. [8] in order to obtain a positive semidefinite gluon propagator. From our data it is difficult to say what would be the behavior of this vertex at very small momenta. However, in one of the kinematical configurations considered here, the three-gluon vertex becomes negative at the smallest nonzero momentum (about 240 MeV). Thus, a possible scenario could be a vertex becoming larger (in absolute value) as the zero momentum limit is approached. Let us note that a positive infrared divergent three-gluon vertex has been recently found in functional studies in three dimensions [11].

The ghost-gluon vertex stays constant and essentially equal to the tree-level value in the range of momenta considered. This is in agreement with various theoretical predictions [10–12] and with numerical results for the 4d case [25,26].

Thus, our results, albeit exploratory, seem to support (at least at the qualitative level) the Gribov-Zwanziger and Kugo-Ojima scenarios of confinement and the central assumptions usually considered in functional methods. In particular, we have shown (see Fig. 7) that the smallest nonzero eigenvalue of the Faddeev-Popov matrix goes to zero in the continuum limit, i.e. a (continuum) Landau configuration should belong to the first Gribov horizon. On the other hand, these results should be taken with caution, as we know that in 3d with the (physical) volumes considered here the true asymptotic infrared region has not been reached yet [18].

We plan to extend this study to larger lattice volumes, in order to explore the far infrared limit. We also plan to consider other gauge groups, especially the physical SU(3) group. Finally, one should consider possible systematic effects related to the existence of Gribov copies.

ACKNOWLEDGMENTS

A. M. was supported by the DFG under Grant No. MA 3935/1-1. A. C. and T. M. were supported by FAPESP (under Grant No. 00/ 05047-5) and by CNPq.

[1] V. N. Gribov, Nucl. Phys. **B139**, 1 (1978).
[2] D. Zwanziger, Nucl. Phys. **B412**, 657 (1994).
[3] D. Zwanziger, Phys. Rev. D **65**, 094039 (2002); **69**, 016002 (2004), and references therein.
[4] D. Zwanziger, Phys. Rev. D **67**, 105001 (2003).
[5] T. Kugo and I. Ojima, Prog. Theor. Phys. Suppl. **66**, 1 (1979); **71**, 1121(E) (1984); T. Kugo, hep-th/9511033.
[6] R. Alkofer and L. von Smekal, Phys. Rep. **353**, 281 (2001), and references therein.
[7] L. von Smekal, A. Hauck, and R. Alkofer Phys. Rev. Lett. **79**, 3591 (1997); Ann. Phys. (N.Y.) **267**, 1 (1998); **269**, 182(E) (1998); C. S. Fischer and R. Alkofer, Phys. Lett. B **536**, 177 (2002); C. S. Fischer, R. Alkofer, and H. Reinhardt, Phys. Rev. D **65**, 094008 (2002).
[8] A. Maas, J. Wambach, B. Grüter, and R. Alkofer, Eur. Phys. J. C **37**, 335 (2004).
[9] H. Gies, Phys. Rev. D **66**, 025006 (2002); C. S. Fischer and H. Gies, J. High Energy Phys. 10 (2004) 048; J. M. Pawlowski, D. F. Litim, S. Nedelko, and L. von Smekal, Phys. Rev. Lett. **93**, 152002 (2004).
[10] R. Alkofer, C. S. Fischer, and F. J. Llanes-Estrada, Phys. Lett. B **611**, 279 (2005).
[11] W. Schleifenbaum, M. Leder, and H. Reinhardt, Phys. Rev. D **73**, 125019 (2006).
[12] W. Schleifenbaum, A. Maas, J. Wambach, and R. Alkofer, Phys. Rev. D **72**, 014017 (2005).
[13] S. Furui and H. Nakajima, Phys. Rev. D **69**, 074505 (2004).

[14] K. Langfeld *et al.*, hep-th/0209173; J. C. R. Bloch, A. Cucchieri, K. Langfeld, and T. Mendes, Nucl. Phys. B, Proc. Suppl. **119**, 736 (2003).
[15] J. C. R. Bloch, A. Cucchieri, K. Langfeld, and T. Mendes, Nucl. Phys. **B687**, 76 (2004).
[16] A. Sternbeck, E. M. Ilgenfritz, M. Müller-Preussker, and A. Schiller, Phys. Rev. D **72**, 014507 (2005).
[17] A. Cucchieri, Phys. Rev. D **60**, 034508 (1999); A. Cucchieri, F. Karsch, and P. Petreczky, Phys. Rev. D **64**, 036001 (2001).
[18] A. Cucchieri, T. Mendes, and A. Taurines, Phys. Rev. D **67**, 091502(R) (2003).
[19] P. J. Silva and O. Oliveira, hep-lat/0511043; M. B. Parappilly *et al.*, hep-lat/0601010.
[20] A. Cucchieri and T. Mendes, Phys. Rev. D **73**, 071502(R) (2006).
[21] P. Boucaud *et al.*, hep-lat/0602006.
[22] C. S. Fischer, B. Gruter, and R. Alkofer, hep-ph/0506053.
[23] P. Boucaud *et al.*, hep-ph/0507104.
[24] C. Lerche and L. von Smekal, Phys. Rev. D **65**, 125006 (2002).
[25] A. Cucchieri, T. Mendes, and A. Mihara, J. High Energy Phys. 12 (2004) 012.
[26] E. M. Ilgenfritz, M. Müller-Preussker, A. Sternbeck, and A. Schiller, hep-lat/0601027.
[27] T. Appelquist and R. D. Pisarski, Phys. Rev. D **23**, 2305 (1981); A. Maas, Mod. Phys. Lett. A **20**, 1797 (2005).
[28] D. Zwanziger, Phys. Rev. D **70**, 094034 (2004).
[29] C. Parrinello, Phys. Rev. D **50**, R4247 (1994).
[30] B. Alles *et al.*, Nucl. Phys. **B502**, 325 (1997).
[31] P. Boucaud *et al.*, J. High Energy Phys. 04 (2000) 006; P. Boucaud *et al.*, J. High Energy Phys. 10 (1998) 017.
[32] A. Sternbeck, E. M. Ilgenfritz, and M. Müller-Preussker, Phys. Rev. D **73**, 014502 (2006).
[33] *Quantum Fields on a Lattice*, edited by I. Montvay and G. Münster, Cambridge Monographs on Mathematical Physics (Cambridge Univ. Press, Cambridge, England, 1994).
[34] S. L. Adler, Phys. Rev. D **23**, 2901 (1981); S. L. Adler, Phys. Rev. D **37**, 458 (1988).
[35] M. Creutz, Phys. Rev. D **21**, 2308 (1980).
[36] A. D. Kennedy and B. J. Pendleton, Phys. Lett. B **156**, 393 (1985).
[37] M. J. Teper, Phys. Rev. D **59**, 014512 (1999); B. Lucini and M. Teper, Phys. Rev. D **66**, 097502 (2002).
[38] A. D. Sokal, "*Functional Integration: Basics and Applications*," Cargèse summer school, 1996 (unpublished); http://citeseer.ifi.unizh.ch/sokal96monte.html.
[39] A. Cucchieri and T. Mendes, Nucl. Phys. **B471**, 263 (1996); Nucl. Phys. B, Proc. Suppl. **53**, 811 (1997).
[40] A. Cucchieri, T. Mendes, G. Travieso, and A. R. Taurines, hep-lat/0308005.
[41] *Lattice Gauge Theories. An Introduction*, edited by H. J. Rothe, Lect. Notes Phys. Vol. 59 (World Scientific, Singapore, 1997).
[42] J. I. Skullerud, D. B. Leinweber, C. Parrinello, and A. G. Williams (UKQCD Collaboration), Nucl. Phys. B, Proc. Suppl. **73**, 626 (1999).
[43] G. P. Lepage and P. B. Mackenzie, Phys. Rev. D **48**, 2250 (1993).
[44] A. Cucchieri and F. Karsch, Nucl. Phys. B, Proc. Suppl. **83**, 357 (2000).
[45] A. Cucchieri, hep-lat/9908050.
[46] P. Boucaud *et al.*, hep-lat/0506031.
[47] A. Cucchieri, Nucl. Phys. **B508**, 353 (1997).
[48] G. Meurant and Z. Strakoš, Acta Numerica **15**, 471, (2006).
[49] A. Cucchieri, T. Mendes, and A. Mihara, Phys. Rev. D **72**, 094505 (2005).
[50] S. Furui and H. Nakajima, Phys. Rev. D **73**, 094506 (2006).
[51] B. N. Parlett, H. Simon, and L. M. Singer, Math. Comput. **38**, 153 (1982); *The Symmetric Eigenvalue Problem*, edited by B. N. Parlett (Prentice Hall, Englewood Cliffs, NJ, 1980).
[52] J. Greensite, Š. Olejník, and D. Zwanziger, J. High Energy Phys. 05 (2005) 070.
[53] J. S. Ball and T. W. Chiu, Phys. Rev. D **22**, 2550 (1980); **23**, 3085(E) (1981).
[54] J. C. Taylor, Nucl. Phys. **B33**, 436 (1971).
[55] A. Cucchieri, A. Maas, and T. Mendes (unpublished).
[56] R. Brun and F. Rademakers, Nucl. Instrum. Methods Phys. Res., Sect. A **389**, 81 (1997).